ACSNANO

www.acsnano.org

ARTICLE

Combined Catalysis for Engineering Bioinspired, Lignin-Based, Long-Lasting, Adhesive, Self-Mending, Antimicrobial Hydrogels

Samson Afewerki,* Xichi Wang, Guillermo U. Ruiz-Esparza, Cheuk-Wai Tai, Xueying Kong, Shengyang Zhou, Ken Welch, Ping Huang, Rhodel Bengtsson, Chao Xu,* and Maria Strømme*

Cite This: https://dx.doi.org/10.1021/acsnano.0c06346

Read Online

ACCESS | Metrics & More | Article Recommendations | Supporting Information

ABSTRACT: The engineering of multifunctional biomaterials using a facile sustainable methodology that follows the principles of green chemistry is still largely unexplored but would be very beneficial to the world. Here, the employment of catalytic reactions in combination with biomass-derived starting materials in the design of biomaterials would promote the development of eco-friendly technologies and sustainable materials. Herein, we disclose the combination of two catalytic cycles (combined catalysis) comprising oxidative decarboxylation and quinone-catechol redox catalysis for engineering lignin-based multifunctional antimicrobial hydrogels. The bioinspired design mimics the catechol chemistry employed by marine mussels in nature. The resultant multifunctional sustainable hydrogels (1) are robust and elastic, (2) have strong antimicrobial activity, (3) are adhesive to skin tissue and various other surfaces, and (4) are able to self-mend. A systematic characterization was carried out to fully elucidate and understand the facile and efficient catalytic strategy and the subsequent multifunctional materials. Electron paramagnetic resonance analysis confirmed the long-lasting quinone-catechol redox environment within the hydrogel system. Initial *in vitro* biocompatibility studies demonstrated the low toxicity of the hydrogels. This proof-of-concept strategy could be developed into an important technological platform for the eco-friendly, bioinspired design of other multifunctional hydrogels and their use in various biomedical and flexible electronic applications.

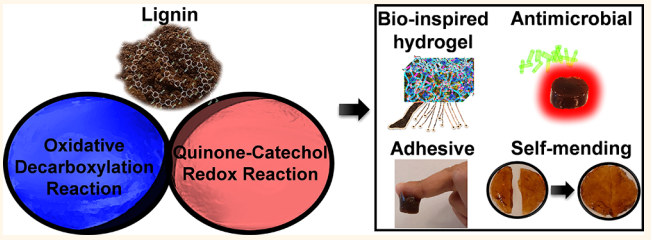

KEYWORDS: *combined catalysis, lignin, bioinspired, antimicrobial, self-healing, hydrogel, adhesive*

The design and engineering of tailor-made materials with diverse functionalities has led to their use in many areas involving various important applications.[1] Nevertheless, the fabrication of these materials using an efficient and facile approach is still a challenge, with several bottlenecks still existing that require further research.[2] Furthermore, our planet and human society as a whole are currently encountering overwhelming challenges. Man-made environmental disturbances such as greenhouse gas emissions have resulted in severe climate change problems,[3,4] and a global health threat based on the prevalence of microbial infections caused by antibiotic-resistant pathogenic micro-organisms has resulted in vastly increased healthcare costs.[5,6] Consequently, the development of novel, innovative green technologies for battling these huge challenges is essential.[7,8] In this context, the employment of catalysis in engineering the desired materials would overcome some of the challenges and promote a more sustainable approach.[9−11] In addition, the employment of biomass as a starting material is considered safer for the environment than fossil-based materials and also provides valorization of waste biomass.[12,13] This helps to promote a "circular economy" approach.[14,15]

Lignin, one of the most abundant sustainable resources on earth, consists of complex polyphenols that contain valuable structural moieties. This makes lignin highly interesting for valorization[16] and use in the design of biomaterials with tissue adhesive[17] and antibacterial properties.[18] The plentiful

Received: July 29, 2020
Accepted: December 4, 2020

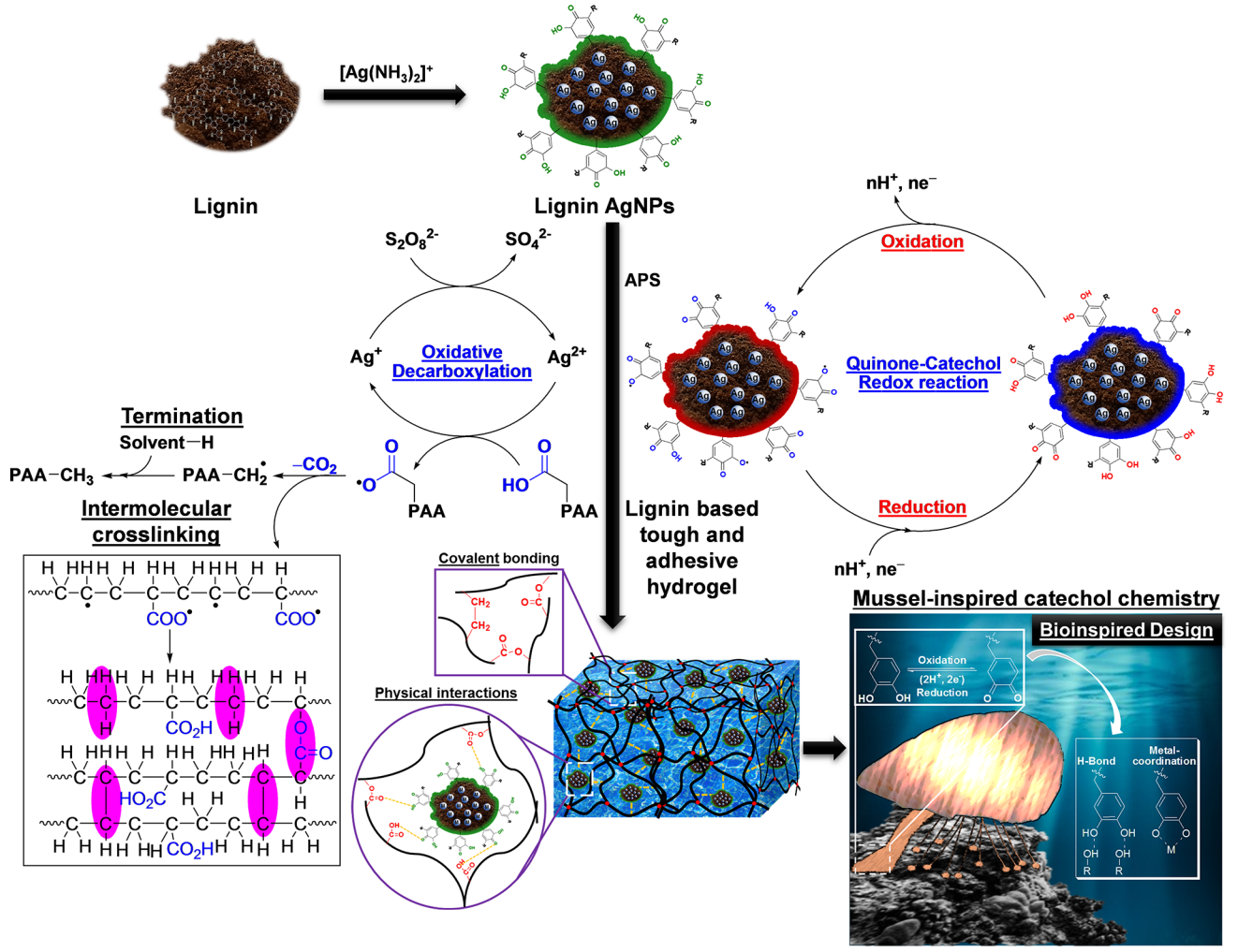

Figure 1. Overview of the catalytic chemical strategy. The bioinspired strategy is based on marine mussel catechol chemistry and the combined oxidative decarboxylation and quinone-catechol redox catalysis reactions used to engineer the lignin-based adhesive antimicrobial hydrogel. AgNPs = silver nanoparticles; APS = ammonium persulfate; PAA = poly(acrylic acid) .

catechol and pyrogallol groups in lignin[19,20] promote many opportunities for covalent or physical interactions with organic or inorganic materials through hydrogen bonding, metal coordination, or hydrophobic and ionic interactions.[21,22] Additional interaction possibilities such as imine or amine-bond formation through a Schiff base reaction or Michael-type addition, respectively, have found an important application in the development of tissue adhesive materials.[17,23,24] In the field of tissue engineering and related biomedical applications, the design of flexible tissue adhesive hydrogels is very important, since these would have potential for use in a broad spectrum of applications such as site-specific drug delivery, treatment of internal bleeding,[23] gluing or sealing tissue to replace surgical sutures,[25] and adhesive patches[26] and applications related to flexible electronics.[27] The development of natural biomaterials with antibacterial properties is particularly desirable in our field of interest, since this would allow the employment of antibiotics to be avoided.[28] With regard to catalysis, the combination of two catalytic cycles in forming new chemical bonds or activation pathways could promote innovative ways to efficiently make use of multifunctional materials.[29]

Scientists have always been captivated by nature and its extraordinarily sophisticated and advanced strategies for engineering highly complex multifunctional materials. Consequently, great effort has been put into mimicking the complex machinery occurring in nature.[30] A perfect example of nature inspiring science is the fascination of researchers around the world with the ability of the marine mussel to adhere to wet surfaces, and the subsequent work aiming to construct high-performance materials with this characteristic.[17] The mechanism underlying wet adhesion is based on multichemical interactions occurring in a protein-rich liquid secreted from the mussel phenol gland;[31] these interactions promote adhesion and cohesion. We were inspired by this work and subsequently developed our objective of designing bioinspired hydrogels using mussel-inspired catechol chemistry, with lignin as the model molecule containing the necessary structures.

In recent work by Gan *et al.*, the use of silver-lignin nanoparticles (Ag-lignin NPs) to trigger dynamic redox catechol chemistry was disclosed.[32,33] The Ag-lignin NPs further generate free radicals that were used to promote the free radical polymerization of monomeric acrylate such as acrylic acid and poly(ethylene glycol) diacrylate to generate a hydrogel with tissue adhesion ability, originating from the lignin within the dynamic redox catechol chemistry.

The intention in this work was to combine two different catalytic reaction cycles (combined catalysis) to engineer a bioinspired lignin-based, tough, adhesive, self-mending, anti-

https://dx.doi.org/10.1021/acsnano.0c06346
ACS Nano XXXX, XXX, XXX−XXX

A

Entry[a]	Polymer[b]	H_2O (mL)	$AgNO_3$ (mL)	APS (1 wt.%)	Lignin 5AgNPs (mL)	Crosslinked hydrogel[c]	Tissue adhesive[d]
1	PAA	1.5		0.5 mL		No	-
2	PAA	1.5	0.5			No	-
3	PAA	1.0	0.5	0.5 mL		Yes	No
4[e]	PAA	1.0	0.5	0.5 mL		Yes	No
5[f]	PAA	1.0	0.5	0.5 mL		Yes	No
6	PAA	1.5			0.5	No	-
7	PAA		0.5		1.5	No	-
8	PAA				2.0	No	-
9	PAA	1.0		0.5 mL	0.5	Yes	Yes
10	PAA	0.5		0.5 mL	1.0	Yes	Yes
11	Alginate	1.0	0.5	0.5 mL		No	-
12	CMC	1.0	0.5	0.5 mL		No	-

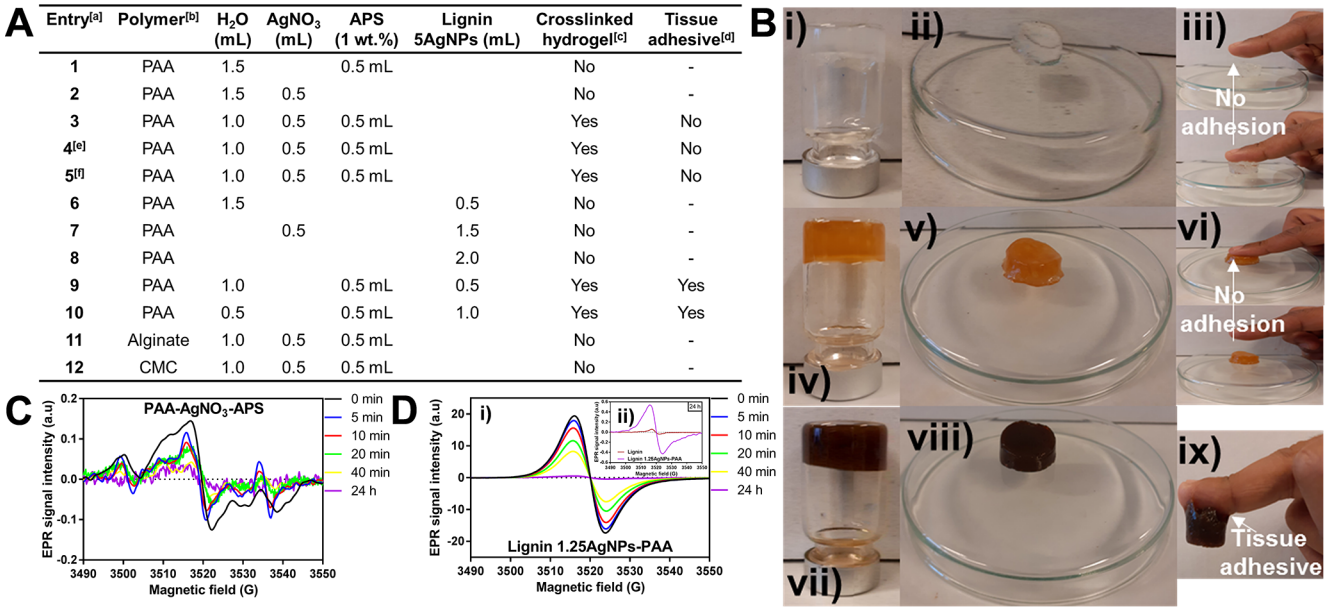

Figure 2. Optimization studies for engineering the multifunctional hydrogel. The screening studies for engineering the lignin-based, cross-linked, tissue adhesive hydrogels. (A) Summary of the parameters that were tested in the screening studies (*e.g.* concentrations and polymers). [a]Reaction conditions: the polymer (20 wt %) was mixed into water and/or lignin AgNPs solution, and APS (0.5 mL, 1 wt %) was added [for some entries, $AgNO_3$ (0.5 mL, 1 wt %) was also added], followed by incubation at room temperature for 1−16 h. The total amount of solvent was 2 mL for all entries. [b]20 wt % of the polymers was prepared to give a final concentration of 10 wt %. [c]The success of the cross-linking was assessed by the formation of a self-standing hydrogel. [d]The initial assessment of the tissue adhesive properties in the screening study was carried out by placing the finger of the researcher onto the cross-linked hydrogel and then lifting it. [e]0.1 mL lignin solution (20 mg/mL) was added. [f]0.2 mL lignin solution (20 mg/mL) was added. (B) The images show the self-standing hydrogels: (i−iii) This PAA hydrogel lacked tissue adhesive properties (A, entry 3); (iv−vi) the addition of lignin alone did not induce tissue adhesion (A, entry 4); and (vii−ix) the addition of lignin AgNPs induced the tissue adhesive properties in the cross-linked hydrogel (A, entry 9). (C) EPR spectra of the reaction for engineering the PAA-based hydrogel at various time points. (D) (i) EPR spectra of the reaction for engineering the lignin 1.25AgNPs-PAA hydrogel at various time points. (ii) The inset shows the spectrum after 24 h compared to the spectrum of lignin. APS = ammonium persulfate; EPR = electron paramagnetic resonance; NPs = nanoparticles; PAA = poly(acrylic acid).

microbial hydrogel (Figure 1). The combined catalysis reactions comprise an oxidative decarboxylation chemical strategy and a quinone-catechol redox reaction, catalyzed by a silver catalyst. The Ag(I)-catalyzed oxidative decarboxylation removes the carbon dioxide (CO_2) moiety from carboxylic (COOH) groups in the presence of ammonium persulfate (APS), which promotes radical reactions (Schemes S1−S4).[34] COOH groups are ubiquitous in nature, and it is therefore of particular interest to develop facile strategies for their functionalization. This strategy has previously been used to cross-link COOH-containing polymers in various systems to provide hydrogels (Scheme S3).[35] The proposed combined catalytic strategy would allow the cross-linking of various bulk materials and polymers postpolymerization without the need of extra modification steps or the use of cross-linking agents.

Moreover, it has earlier been demonstrated that lignin can be employed as a sustainable material for preparing various metal-based NPs by acting as both a reducing and a stabilizing agent, thus simultaneously generating NPs and partly activating the lignin catechol functionalities (Figure 1).[36−40]

RESULTS AND DISCUSSION

Engineering of Lignin-Based Tissue Adhesive Hydrogels. The devised strategy is depicted in Figure 1. The silver nanoparticles (AgNPs) are generated by mixing the silver ammonia ($[Ag(NH_3)_2]^+$) complex with the green reducing agent lignin, resulting in lignin AgNPs (for more details see Supporting Information). Subsequent addition of the radical generator APS and the polymer poly(acrylic acid) (PAA) promotes the dual activation of the quinone-catechol redox reaction, which provides the adhesive properties of the hydrogel, and simultaneously the catalytic oxidative decarboxylation reaction, generating a self-standing cross-linked hydrogel. Nevertheless, one limitation that should not be ruled out is the ability of lignin and the corresponding quinones reacting as efficient radical scavengers. In the case of this process occurring in an adequate amount, the intermolecular cross-linking would most likely by inhibited, thus leading to the failure of promoting a self-standing hydrogel.[41,42] The strategy was evaluated by a thorough proof-of-concept screening study in order to provide a successful cross-linked hydrogel with tissue adhesive properties. Initial attempts to cross-link the PAA (1 mL, 20 wt %) with catalytic amounts of either the radical initiator APS (0.5 mL, 1 wt %) or the catalyst silver nitrate ($AgNO_3$) (0.5 mL, 1 wt %) did not provide any successful cross-linked self-standing hydrogels (Figure 2A, entries 1 and 2). While APS does generate radicals, their lifetimes are normally very short without a regenerative environment or catalyst, leading to decomposition of the persulfate radicals by reaction with water.[43] The electron paramagnetic resonance (EPR) analysis did not detect the radicals generated (Figure S1A). When both the radical generator APS and the regenerative catalyst $AgNO_3$ were used together, a cross-linked, self-standing PAA-based hydrogel was produced (Figure 2A, entry 3). However, the hydrogel material did not show any tissue adhesive properties (Figure 2B, i−iii)). The generation of $^{\bullet}CH_2$ radicals (Figure 2C) was confirmed

https://dx.doi.org/10.1021/acsnano.0c06346
ACS Nano XXXX, XXX, XXX−XXX

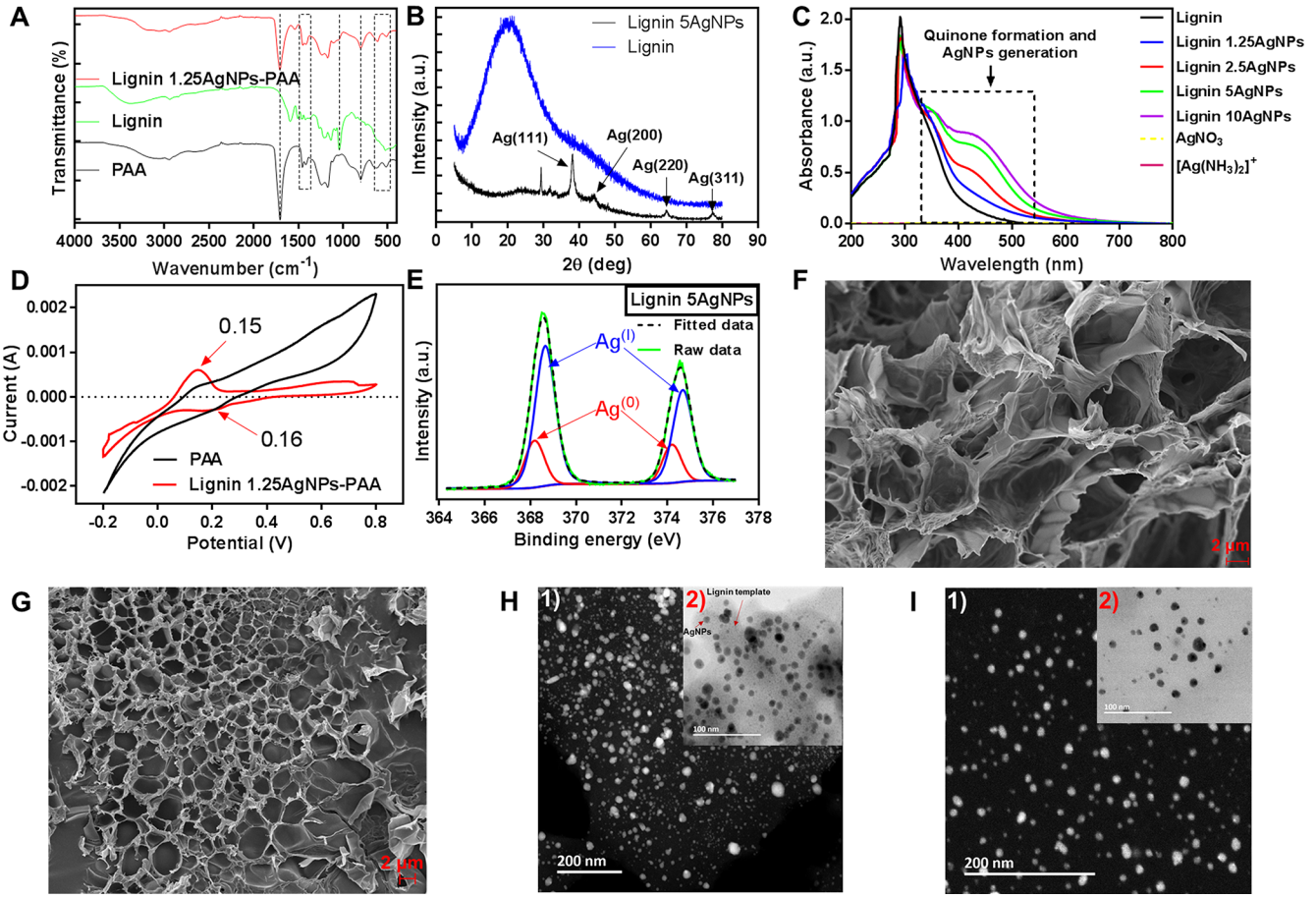

Figure 3. Characterization of the lignin AgNPs-based materials. (A) FTIR of the lignin 1.25AgNPs-PAA, lignin, and PAA samples. (B) XRD patterns for the lignin and lignin 5AgNPs samples. (C) UV−vis spectra of lignin, ligninxAgNPs with various silver concentrations (*x*), $AgNO_3$, and $[(Ag(NH_3)_2)^+]$. (D) CV investigation of the PAA and lignin 1.25AgNPs-PAA samples with the materials as the working electrodes in a solution containing 2 wt % PAA and 1 wt % ammonium persulfate over one cycle, with a scanning speed of 5 mV/s and the potential given *versus* Ag/AgCl. (E) High-resolution Ag 3d X-ray photoelectron spectrum for the lignin 5AgNPs sample and the deconvolution results. (F) SEM image of the cross-linked PAA with a scale bar of 2 μm. (G) SEM image of the lignin 1.25AgNPs-PAA hydrogel sample with a scale bar of 2 μm. (H) STEM analysis confirmed the presence of the AgNPs in the lignin 5AgNPs sample: (1) HAADF STEM image with a scale bar of 200 nm and (2) BF STEM image with a scale bar of 100 nm. (I) STEM analysis confirmed the presence of the AgNPs in the lignin 1.25AgNPs-PAA sample: (1) HAADF STEM image with a scale bar of 200 nm and (2) BF STEM image with a scale bar of 100 nm. FTIR = Fourier transform infrared spectroscopy; SEM = scanning electron microscopy; STEM = scanning transmission electron microscopy; HAADF = high-angle annular dark-field; BF = bright-field.

by EPR simulation (Figure S2). The observable time in tens of minutes, together with the inhomogeneous feature of the entire spectrum, strongly suggests that the radical signals are under accumulation as a result of regeneration which only can occur under a reductive environment. The radicals vanished after about 40 min once the polymerization process was accomplished (Figure 2C). In an effort to induce tissue adhesive properties, lignin was added to the PAA-based hydrogel (Figure 2A, entries 4 and 5), but this also failed to promote tissue adhesion (Figures 2B, iv−vi and S3A). Although lignin can provide a reductive environment and generate some radicals, they are not long-lived nor sufficient to promote the reversible quinone-catechol redox reaction (Figure S1B,C). We then premixed the lignin with the $[Ag(NH_3)_2]^+$ in order to activate the lignin into its oxidized form (quinone-catechol redox reaction), concurrently generating AgNPs. The lignin 5AgNPs (final concentration of silver was 5 mg/mL) were then used in the hydrogel formation reaction. Using the lignin 5AgNPs alone or in combination with $AgNO_3$ did not provide any cross-linked hydrogels (Figure 2A, entries 6−8). However, to our delight, when PAA was mixed with the lignin 5AgNPs and APS, a successful cross-linked tissue adhesive hydrogel resulted [Figure 2A, entry 9 (lignin 1.25AgNPs-PAA) and entry 10 (lignin 2.5AgNPs-PAA), and Figures 2B, vii−ix and S3B]. These results underline the importance of having both the oxidized form of lignin and the quinone-catechol redox reaction to induce the tissue adhesive properties. It has previously been demonstrated that lignin becomes strongly tissue adhesive by the activation of a redox catechol process triggered by silver.[32] Fascinatingly, even after 24 h, the lignin 1.25AgNPs-PAA sample chemical process was still active within the hydrogel, as confirmed by EPR spectra, demonstrating the presence of long-lasting radicals from the regenerative silver, with lignin stabilization through the reversible redox-catechol reaction (Figures 2D and S1E). When other polymer-containing carboxylic groups, such as alginate and carboxymethyl cellulose (CMC), were investigated, successful cross-linked hydrogels were not produced (Figure 2A, entries 11 and 12). This could have been the result of fewer carboxylic groups in their structures,

https://dx.doi.org/10.1021/acsnano.0c06346
ACS Nano XXXX, XXX, XXX−XXX

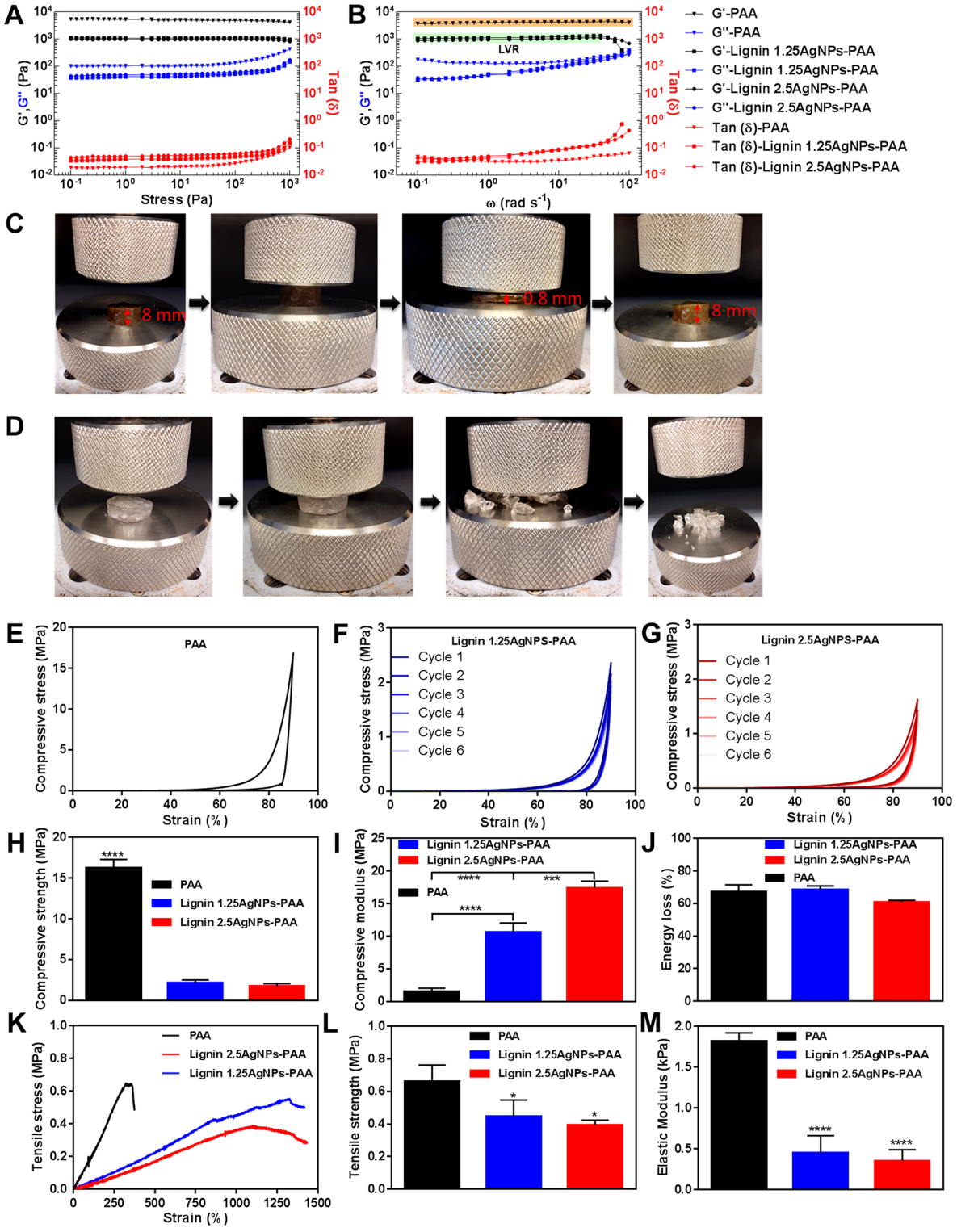

Figure 4. Rheological and mechanical properties of the various engineered hydrogels obtained. (A) The oscillatory stress sweep and (B) the angular frequency (ω) sweep. The orange and green areas indicate the linear viscoelastic region. (C) The lignin 1.25AgNPs-PAA hydrogel compressed to 90% of its height and immediately recovered. (D) The PAA hydrogel was destroyed by compression. (E) Representative compression stress−strain curves of the PAA hydrogel. Cyclic compression stress−strain curves of (F) the lignin 1.25AgNPs-PAA hydrogel and (G) the lignin 2.5AgNPs-PAA hydrogel. Graphs of various hydrogels showing (H) compressive strength, (I) compressive modulus, and (J) energy loss data. Graphs of tensile tests of the various hydrogels showing (K) representative tensile stress−strain curves, (L) ultimate tensile strength, and (M) elastic modulus. Values are means ± SD, generated by one-way ANOVA followed by Tukey's multiple comparison test, $N = 5$. (*) $p < 0.05$, (***) $p < 0.005$, (****) $p < 0.001$, indicating statistically significant differences. NPs = nanoparticles; PAA = poly(acrylic acid) ; LVR = linear viscoelastic region; SD = standard deviation.

https://dx.doi.org/10.1021/acsnano.0c06346
ACS Nano XXXX, XXX, XXX−XXX

since the degree of functionality plays an important role in promoting cross-linking and devising a successful hydrogel.[44,45]

Various other lignin-based metal NPs were also prepared as a result of the ability of lignin as a green reducing agent to transform metal salts into NPs.[46] These metal NPs were successfully produced in various sizes: PdNPs 41.5 ± 2.35 nm (polydispersity index (PDI) = 0.363); AgNPs 43.3 ± 0.32 nm (PDI = 0.727); NiNPs 165.9 ± 2.61 nm (PDI = 0.411); CuNPs 238.1 ± 1.21 nm (PDI = 0.223); FeNPs 245.2 ± 1.31 nm (PDI = 0.264); ZnNPs 248.9 ± 0.81 nm (PDI = 0.279) (Figure S4A). The NPs were evaluated in the combined oxidative decarboxylation and quinone-catechol redox catalysis reaction in an attempt to engineer lignin-based cross-linked, tissue adhesive hydrogels. The various metal salts in combination with APS did not provide any cross-linked hydrogel in the oxidative decarboxylation reaction (Table S1, entries 1, 5, 9, 13, and 17).[47] However, their corresponding lignin-based metal NPs (PdNPs, CuNPs, FeNPs, NiNPs, and ZnNPs) in combination with APS generated self-standing, tissue adhesive hydrogels (Table S1, entries 3−4, 7−8, 11−12, 15−16, and 19−20, and Figure S3C−L). The mechanism for the hydrogel formation could plausibly involve the radicals generated from the lignin moiety promoting the cross-linking[32,48] or perhaps the PAA forming a cross-linked network with the metal ions (Cu^{2+}, Ni^{2+}, Zn^{2+}, and Fe^{3+}), providing self-standing hydrogels.[49,50] In addition, ligninxAgNPs containing varying concentrations of silver (x mg/mL) were prepared, resulting in NPs of various sizes (28.7−65.2 nm). Intriguingly, the sizes of the NPs decreased with increasing amounts of silver (Figure S4B).

Characterization. A thorough characterization of the engineered materials was carried out. The lignin 5AgNPs and the lignin 1.25AgNPs-PAA samples were characterized by Fourier transform infrared spectroscopy (FTIR) analysis, as depicted in Figures 3A and S5. The presence of the lignin moiety in the lignin 5AgNPs and lignin 1.25AgNPs-PAA was clearly detected from the aromatic ring bands at ∼1590 and ∼1505 cm^{-1} and the C−O deformation of the methoxy groups at ∼1040 cm^{-1}.[38,46,51] Peaks at ∼3414 and ∼1265 cm^{-1} from the phenolic hydroxyl (−OH) groups of lignin were also observed. These peaks either decreased in intensity or disappeared after the lignin oxidation by silver (lignin 5AgNPs and lignin 1.25AgNPs-PAA), indicating that the catechol groups of the lignin were oxidized to quinone groups by the silver ions (Ag^+). The presence of the PAA moiety in the lignin 1.25AgNPs-PAA sample was confirmed by the presence of the carbonyl group (C═O) at ∼1700 cm^{-1}, C−H at ∼2940 cm^{-1}, C−O−H bending vibration at ∼1450 and ∼1415 cm^{-1}, O−H bending and C−O stretching at ∼1240 and ∼1165 cm^{-1}, and the peaks at ∼630 and ∼510 cm^{-1}, corresponding to PAA.[52,53] The lignin 5AgNPs were further characterized by powder X-ray diffraction (XRD) analysis (Figure 3B). The characteristic main peaks of the AgNPs were seen at $2\theta \approx 38.2°$, 44.2°, 64.4°, and 77.3°, corresponding to the (111), (200), (220), and (311) planes. One unsigned peak at 29.4° was also detected; this might correspond to organic compounds in the lignin as has been observed previously.[54] UV−vis analysis of the generated lignin-based AgNPs confirmed a quinone formation and the generation of AgNPs, which increased with increased amounts of silver added to the reaction mixture, indicating that higher amounts of silver promoted the oxidation of the catechol and methoxy groups on lignin to quinone groups (Figure 3C).[55−57] Cyclic voltammetry (CV) experiments confirmed the catechol-quinone reaction in the system (Figure S6). The reversible redox reaction of the lignin 1.25AgNPs-PAA sample was observed at 0.15 and 0.16 V *versus* Ag/AgCl, but was not observed for the PAA sample (Figure 3D). These initial findings confirm the oxidation of lignin to form quinone groups during the course of the CV analysis.[58,59] The presence of the redox reaction was also confirmed by X-ray photoelectron spectroscopy (XPS), by which both Ag^+ and AgNPs were detected in the lignin 5AgNPs sample (Figure 3E). In addition, the morphology of the materials was analyzed in a scanning electron microscope (SEM). The PAA material had a three-dimensional (3D) networked microstructure with large pores (Figure 3F), while the lignin 1.25AgNPs-PAA sample had smaller interconnected pores that were formed through a chemical cross-linking of the PAA and further interactions with the lignin and AgNPs (Figure 3G). Scanning transmission electron microscopy (STEM) analysis of the lignin 5AgNPs demonstrated homogeneously distributed AgNPs of ∼10 nm in diameter (Figure 3H). The AgNPs were also detected within the corresponding hydrogel (lignin 1.25AgNPs-PAA) without any changes to their morphology or size, indicating that the mild oxidative decarboxylation cross-linking step did not have any negative impact on the AgNPs morphology (Figure 3I).

Evaluation of the Mechanical Properties. The viscoelastic properties of the cross-linked hydrogels were further evaluated using an oscillatory sweep with an oscillation stress of 0.1−1000 Pa and frequency of 1 Hz, and angular frequency (ω) sweep at 0.1−100 rad s^{-1} and 10 Pa, recording the storage (G') and loss modulus (G''). All of the G' values for the various samples were stress independent (Figure 4A); however, the lignin 1.25AgNPs-PAA and lignin 2.5AgNPs-PAA samples showed frequency dependence, since they displayed a linear viscoelastic region of up to $G' \sim 1176$ Pa at $\omega \sim 50$ rad s^{-1} (lignin 1.25AgNPs-PAA) and $G' \sim 1045$ Pa at $\omega \sim 63$ rad s^{-1} (lignin 2.5AgNPs-PAA) (Figure 4B, green area) followed by a decrease in G'. The PAA hydrogel displayed the greatest strength and mechanical rigidity (*i.e.*, it was less flexible), while the lignin 1.25AgNPs-PAA and lignin 2.5AgNPs-PAA samples had similar gel strengths [*e.g.*, at a stress value of 10 Pa $G' \sim 5090$ Pa (PAA), $G' \sim 1101$ Pa (lignin 1.25AgNPs-PAA) and $G' \sim 983$ Pa (lignin 2.5AgNPs-PAA)] (Figure 4A). The higher storage modulus of the PAA can also be translated to a higher degree of cross-linking.[60] Moreover, the crossover points between G' and G'' (the gel point; $\tan(\delta) = 1$) were never observed under the evaluated rheological conditions. This was confirmed in the $\tan(\delta)$ graphs, with $\tan(\delta) < 1$ indicating that the structure of the hydrogels was dominated by their elastic behavior more than their viscosity.[61] The mechanical evaluation based on compression testing demonstrated the impact of incorporating the activated lignin (quinone-catechol redox activation) within the hydrogel system, which provided a speedy recovery (compressed to 90% of its height and immediately recovered) (Figure 4C). The absence of the lignin component in the hydrogel (PAA alone) was not associated with any recovery; the sample was brittle and was immediately destroyed by the compression (Figure 4D). These phenomena were also observed in the cyclic compression tests, where lignin-based hydrogels were compressed during six consecutive cycles and still retained their original structure (Figures 4E−G). Moreover, despite the enhanced mechanical strength of the hydrogel in the absence of lignin (from the

https://dx.doi.org/10.1021/acsnano.0c06346
ACS Nano XXXX, XXX, XXX−XXX

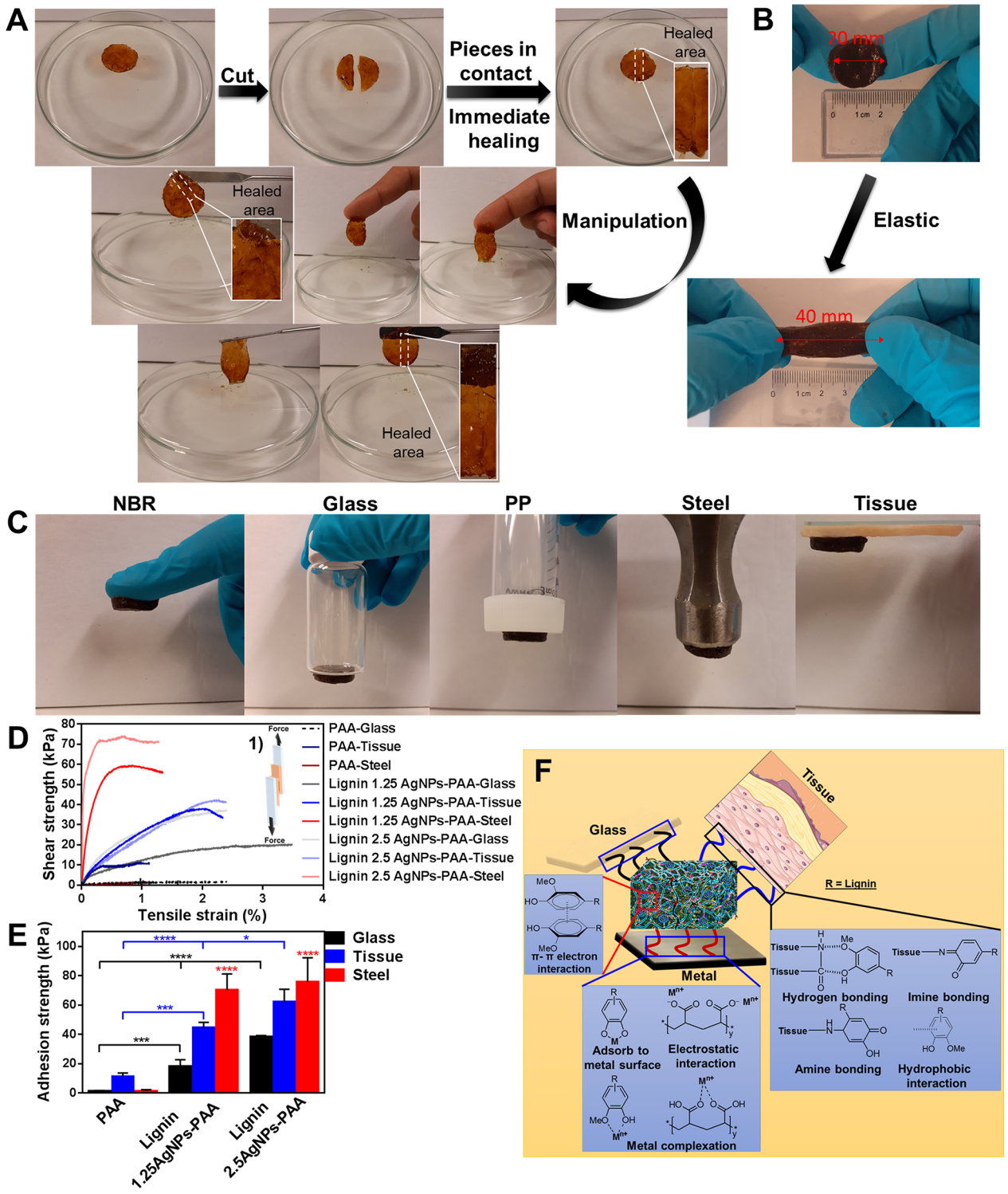

Figure 5. Evaluation of the self-mending and adhesion properties. (A) Images demonstrating the self-mending properties of the engineered hydrogel. After the hydrogel was cut and the pieces put back into contact, there was immediate self-mending. (B) Image demonstrating the stretchability of the engineered lignin-based hydrogel. (C) The adhesive properties of the devised hydrogels on various surfaces such as nitrile butadiene rubber (NBR), glass, polypropylene (PP), steel, and tissue (porcine skin). A standard lap shear test was employed to determine the shear and adhesive strengths. (D) Representative stress−strain curves from the lap shear test: (D1) Illustration of the adhesion tests performed by applying the hydrogel onto various surfaces and subsequently carrying out a lap shear test. (E) Graph of the average adhesion strength. Values are means ± SD, generated by one-way ANOVA followed by Tukey's multiple comparison test, $N = 5$. (*) $p < 0.05$, (***) $p < 0.005$, (****) $p < 0.001$, indicating statistically significant differences. (F) An overview of the different chemical interactions between the devised hydrogel and various surfaces, illustrating strong adhesive properties derived from biomimicry of marine mussel-inspired catechol chemistry. NPs = nanoparticles; PAA = poly(acrylic acid); SD = standard deviation.

https://dx.doi.org/10.1021/acsnano.0c06346
ACS Nano XXXX, XXX, XXX−XXX

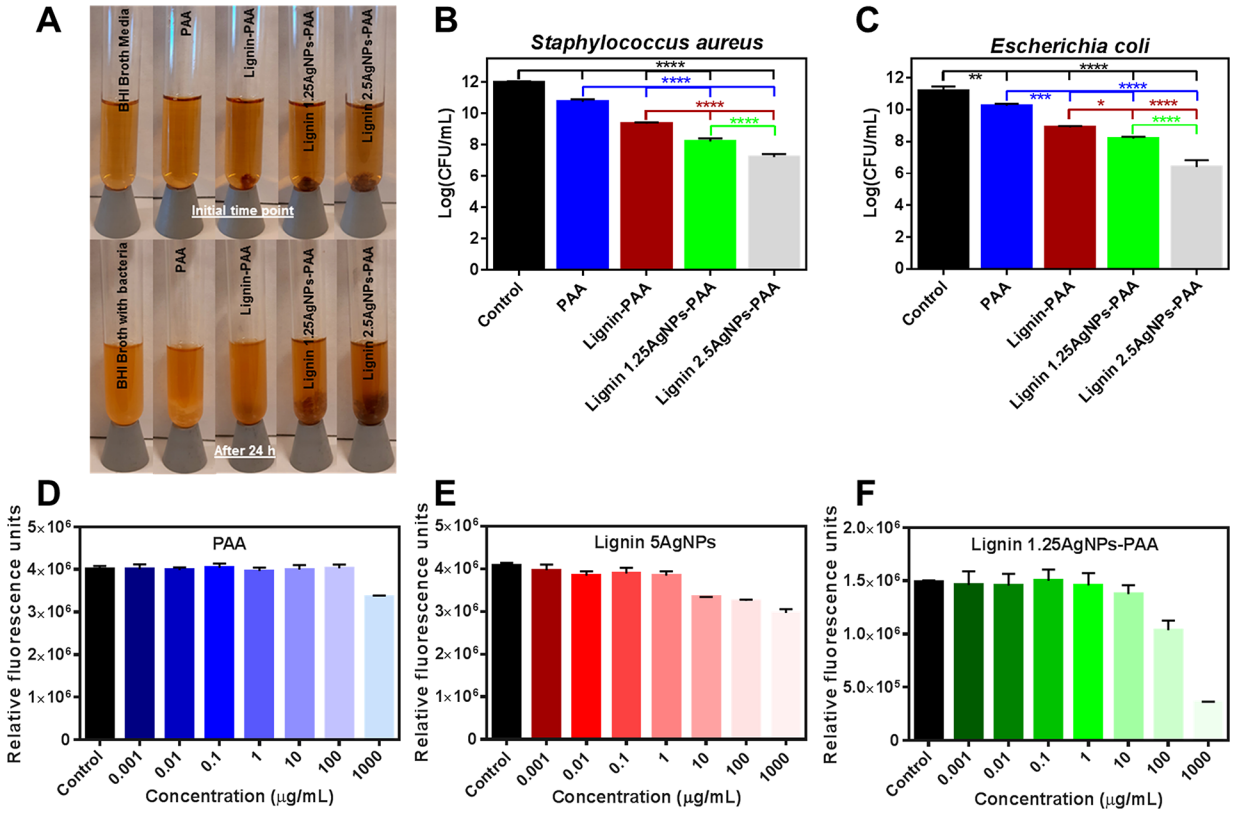

Figure 6. Antibacterial activity of the engineered hydrogels against *S. aureus* and *E. coli*. (A) Images demonstrating the solutions of the bacteria and hydrogels at the initial time point and after 24 h. Number of CFUs of (B) *S. aureus* and (C) *E. coli* after 24 h incubation with the various hydrogels. Values are means ± SD, test of statistical significance generated by one-way ANOVA followed by Tukey's multiple comparison test, $N = 3$. (*) $p < 0.05$, (**) $p < 0.01$, (***) $p < 0.005$, (****) $p < 0.001$. The cytotoxicity determinations for the various compositions were carried out using NIH 3T3 fibroblasts, after 48 h of incubation with increasing sample concentrations (0.001−1000 μg/mL). (D) Cell viability of PAA. (E) Cell viability of lignin 5AgNPs. (F) Cell viability of lignin 1.25AgNPs-PAA. The data are represented as means ± SD; $N = 5$. NPs = nanoparticles; PAA = poly(acrylic acid); SD = standard deviation; CFU = colony-forming unit.

compression stress data) (Figure 4H), the compressive modulus for the lignin-based hydrogels was higher (demonstrating that they are easier to deform and manipulate, which is important for applications such as flexible electronics and biomedical use) (Figure 4I).[62] Furthermore, the energy loss of a viscoelastic biomaterial is an important parameter when mimicking or understanding the processes in native tissues, since tissues and organs are viscoelastic, thus providing information about the energy stored and dissipated during deformation or work.[63] Despite the high energy dissipated by the engineered hydrogels during the compression tests (PAA ∼ 67%, lignin 1.25AgNPs-PAA ∼ 68%, and lignin 2.5AgNPs-PAA ∼ 61%), the lignin-based hydrogels recovered over several cycles (tested for six cycles) without the irreversible structural damage that was seen with the PAA hydrogel (which was deformed after one cycle) (Figure 4J). The ability of the hydrogels to recover to their original structure after repeated breakage and deformation originates from the dynamic chemistry and physical interactions *via* hydrogen bonds and hydrophobic interactions within the hydrogels.[64,65] Figure 4K depicts representative tensile stress−strain curves for various hydrogels. The maximum tensile strain significantly decreased for the lignin-based hydrogels (lignin 1.25AgNPs-PAA ∼ 1260% and lignin 2.5AgNPs-PAA ∼ 1110%) compared to the PPA hydrogel (∼350%). The tensile strength and elastic modulus was higher for the PAA hydrogel than for the lignin-based hydrogels, demonstrating that the lignin-based hydrogels had a greater resistance and were more stretchable/elastic (Figure 4L,M).[62] The toughness and high resilience of the lignin-based hydrogels are associated with the interpenetrating network within the hydrogels through various covalent bonds (covalent bonding through oxidative decarboxylation reaction) and noncovalent interactions (reversible quinone-catechol redox reaction resulting in hydrogen bonding, metal coordination, and hydrophobic- and ionic-based interactions) (Figure 1).

Self-Mending and Tissue Adhesion Properties. The incorporation of activated lignin allowed the quinone-catechol redox reaction to promote physical interactions, thus providing recoverability and also promoting a self-mending ability. As illustrated in Figure 5A, the lignin-based hydrogel demonstrated fast self-mending. After cutting the gel and putting the pieces in contact with each other again, they immediately fused back to the original structure. The self-mending ability of the hydrogels was further quantified through mechanical testing, demonstrating that the hydrogels displayed a 56% (lignin 1.25AgNPs-PAA) and 70% (lignin 2.5AgNPs-PAA) mending efficiency, respectively (Figure S7A). Moreover, the toughness and elasticity of the lignin-based hydrogel was demonstrated by stretching the gel samples (Figures 5B and S7B). The initial screening study demonstrated that the incorporation of activated lignin augmented the tissue adhesion properties of the hydrogel formulations (Figure 2B). The hydrogels also demonstrated the ability to adhere to various surfaces such as

https://dx.doi.org/10.1021/acsnano.0c06346
ACS Nano XXXX, XXX, XXX−XXX

tissue (porcine skin), rubber (nitrile butadiene rubber), glass, polypropylene and steel (Figure 5C). This adhesion to various surfaces was further evaluated using a standard lap shear test to measure the shear strength, based on the ASTM F2255-05 standard and employing a Shimadzu mechanical tester (Figures 5D and S8). When the adhesion to various surfaces (glass, tissue and steel) was quantified, it was found that the PAA hydrogel was minimally adhesive (glass ∼ 1.4, tissue ∼ 11.3 and steel ∼ 1.3 kPa), while the lignin-based hydrogels demonstrated significantly enhanced adhesion to the various surfaces (lignin 1.25AgNPs-PAA: glass ∼ 18.2, tissue ∼ 44.5 and steel ∼ 70.4 kPa; lignin 2.5AgNPs-PAA: glass ∼ 38.2, tissue ∼ 62.4 and steel ∼ 75.9 kPa) (Figure 5E). In general, the order of adhesive ability from most to least adhesive for the hydrogels was steel, tissue, and last glass. In addition, the lignin with increased AgNPs content (lignin 2.5AgNPs-PAA) showed an enhanced adhesion because of the increased quinone-catechol redox reaction activated by the silver (Figure 5E). The superior adhesion of the engineered lignin-based hydrogels to various surfaces is the result of a biomimicry-based adhesive (mussel-inspired catechol chemistry). This adhesive is widely found in creatures such as sandcastle worms and mussels that are rich in catechol groups, allowing an abundance of interaction possibilities.[66] Figure 5F illustrates some of the chemical interactions between the devised hydrogel and the various surfaces, including hydrogen, imine, and amide bonding to tissues, hydrophobic and $\pi-\pi$ interactions, adsorption to metal surfaces, formation of metal complexes, and electrostatic interactions promoting strong adhesion.

Antibacterial Activity. The antibacterial activity of the engineered hydrogels was evaluated in tests using Gram-positive *Staphylococcus aureus* (*S. aureus*) and Gram-negative *Escherichia coli* (*E. coli*). Figure 6A shows images of the bacterial solutions with the hydrogels at the initial time point and after 24 h of incubation. Compared to the control, all of the hydrogels displayed antibacterial activity (the PAA hydrogel antibacterial activity was probably the result of the presence of Ag^+ within the hydrogel). The incorporation of lignin alone into the hydrogel system also resulted in antibacterial activity (compared to PAA and lignin-PAA hydrogels) with 25.0× (*S. aureus*) and 22.7× (*E. coli*) fewer bacteria, corresponding to 1.40- and 1.36-log reductions, respectively.[18] Furthermore, synergistic antibacterial performance was observed when lignin and AgNPs were combined, providing significantly greater reductions in bacterial counts relative to PAA, with 343.8× (2.54-log reduction, *S. aureus*) and 116.7× (2.07-log reduction, *E. coli*) fewer bacteria for the lignin 1.25AgNPs-PAA sample and 3437.8× (3.54-log reduction, *S. aureus*) and 6999.4× (3.85- log reduction, *E. coli*) fewer bacteria for the lignin 2.5AgNPs-PAA sample (Figure 6B,C, groups lignin 1.25AgNPs-PAA and lignin 2.5AgNPs-PAA). The lignin 2.5AgNPs-PAA sample, which contained twice as much silver as the lignin 1.25AgNPs-PAA sample, had significantly enhanced activity compared to the lignin 1.25AgNPs-PAA sample (10.0× fewer bacteria with 1-log reduction, *S. aureus*; and 60.0× fewer bacteria with 1.79-log reduction, *E. coli*). An elution-based antibacterial test was also carried out, and the hydrogels were incubated in bacterial media for 24 h under shaking, at which point they were removed and the solution was tested for antibacterial activity. These experiments demonstrated that the materials released from the hydrogels were strongly antibacterial (Figure S9). Actually, the majority of the antibacterial effect arose from the materials eluted from the hydrogels, for instance, the lignin 2.5AgNPs-PAA group resulted in only 6.2× fewer bacteria with 0.79-log reduction (*E. coli*) compared to the same sample in the elution test (Figures 6C and S9). Overall, the results indicated that the engineered materials efficiently and significantly inhibited both Gram-positive and Gram-negative bacteria. Furthermore, in order to understand the antimicrobial activity promoted by the Ag^+ within the hydrogels, a release study was performed. As demonstrated in Figure S10, an initial burst release of Ag^+ was observed during the first hour (PAA: ∼ 24%, lignin PAA: ∼ 23%, lignin 1.25AgNPs PAA: ∼ 21%, lignin 2.5AgNPs PAA: ∼ 32%) and about 65−77% was released after 24 h (PAA: ∼ 65%, lignin PAA: ∼ 65%, lignin 1.25AgNPs PAA: ∼ 77%, lignin 2.5AgNPs PAA: ∼ 68%), followed by a sustained release for up to 9 days.

Cytotoxicity Assessments. The biocompatibility of the engineered hydrogels was evaluated in a cell viability assay using 3T3 fibroblasts treated with increasing concentrations (0.001−1000 μg/mL) of PAA, lignin 5AgNPs, lignin 10AgNPs, lignin 1.25AgNPs-PAA, and lignin 2.5AgNPs-PAA. The PAA, lignin 5AgNPs, and lignin 10AgNP samples had good cell compatibility at the concentration ranges evaluated; however, the cell viability decreased for the lignin 1.25AgNPs-PAA (to 70% at 100 μg/mL and 28% at 1000 μg/mL) and the lignin 2.5AgNPs-PAA (to 24% at both 100 and 1000 μg/mL) (Figures 6D−F and S11).

CONCLUSION

In this report, we have presented a facile, combined catalytic, eco-friendly process for engineering multifunctional, bioinspired, lignin-based, tough, self-mending, antimicrobial hydrogels. The combined catalysis involved merging the catalytic cycle of the oxidative decarboxylation reaction, which provided chemical cross-linking to the hydrogel, with a quinone-catechol redox catalysis reaction, which promoted physical cross-linking in the hydrogels. The design rationale and the results of the various experiments confirm the importance of activating both the catalytic cycles in order to engineer a self-standing, tissue-adhesive, multifunctional hydrogel. The use of a biomimicry approach (based on marine mussel-inspired catechol chemistry), which led to the incorporation of lignin and the quinone-catechol redox reaction in the hydrogels, resulted in the self-mending properties and the ability to adhere to various surfaces as the result of various chemical interactions between the hydrogel and the surfaces. Importantly, the EPR analysis confirmed a long-lasting quinone-catechol redox environment within the hydrogel system. In the absence of the quinone-catechol redox activations, the hydrogel lost its adhesive and self-mending properties (as shown by the adhesion and compression experiments). In addition, the material showed strong synergistic antibacterial activity against both Gram-positive (*S. aureus*) and Gram-negative (*E. coli*) bacteria, with significant bacterial reductions as the result of the concurrent presence of lignin and AgNPs. The initial *in vitro* viability studies also demonstrated a low toxicity from the engineered hydrogels. Nevertheless, biocompatibility is a parameter that can be further adjusted by altering the lignin and AgNPs concentrations. All the materials demonstrated good compatibility (up to 100 μg/mL), despite the high concentrations of lignin and the presence of AgNPs in the lignin AgNPs-PAA hydrogels. We believe that this technology involving the combination of two catalytic cycles, which promoted innovative chemical reactions, activation modes, and material

https://dx.doi.org/10.1021/acsnano.0c06346
ACS Nano XXXX, XXX, XXX−XXX

properties, has great potential, where the single catalytic cycle failed. In particular, the employment of this technology is notable for its potential in the sustainable design of polymeric systems for cross-linking and formation of hydrogels in a facile and green approach. This strategy will promote innovative chemical approaches for the design of other combined catalytic systems for engineering multifunctional hydrogels. These hydrogels could be potential candidates for various applications, including flexible electronic systems and dressings for infected wounds.

EXPERIMENTAL SECTION

Materials. The following chemicals were purchased from Sigma-Aldrich (St. Louis, MO, USA): poly(acrylic acid) (PAA) (molecular weight (Mw) *ca.* 1,250,000), alkaline lignin (lignin, kraft low sulfonate content), silver nitrate ($AgNO_3$), ammonium persulfate (APS), palladium acetate ($Pd(OAc)_2$) 98%, iron(III) perchlorate hydrate ($Fe(ClO_4)_3)\cdot xH_2O$, and copper(II) nitrate hemi(pentahydrate) ($Cu(NO_3)_2\cdot 2.5H_2O$) (ACS reagent, ≥99.99%). Nickel(II) nitrate hexahydrate 98% ($Ni(NO_3)_2\cdot 6H_2O$) and zinc nitrate hexahydrate 99% ($Zn(NO_3)_2\cdot 6H_2O$) were purchased from Alfa Aesar. Brain heart infusion broth (BHI broth, for microbiology) was obtained from VWR Chemicals, and agar (bacteriological grade) was obtained from VWR Life Science.

Procedure for Preparing the Lignin *x*AgNPs. The lignin AgNPs were prepared following the methods in a previous report with minor modifications.[36] An aqueous solution of 20 mg/mL lignin was prepared by adding the lignin (100 mg) to deionized (DI) water (5 mL) and vortexing and sonicating until it was fully dissolved. In parallel, $AgNO_3$ [100 mg (for preparing 10AgNPs), 50 mg (for 5AgNPs), 25 mg (for 2.5AgNPs), or 12.5 mg (for 1.25AgNPs)] was dissolved in DI water (4 mL), and 1 mL aqueous ammonium solution was added (5 M). The lignin solution was added dropwise to the $AgNO_3$ solution and stirred at room temperature for 1 h.

Procedure for Preparing the Lignin 5PdNPs.[37,38] The lignin PdNPs were prepared following the methods in a previous report with minor modifications. An aqueous solution of 20 mg/mL lignin was prepared by adding the lignin (100 mg) to DI water (5 mL) and vortexing and sonicating until it was fully dissolved. In parallel, $Pd(OAc)_2$ (50 mg) was dissolved in acetone (5 mL). The lignin solution was added dropwise to the $Pd(OAc)_2$ solution, heated to 95 °C, and stirred for 3 h.

Preparation of the Lignin 5CuNPs.[39] The lignin CuNPs were prepared following the methods in a previous report with minor modifications. An aqueous solution of 20 mg/mL lignin was prepared by adding the lignin (100 mg) to DI water (5 mL) and vortexing and sonicating until it was fully dissolved. In parallel, $Cu(NO_3)_2\cdot 2.5H_2O$ (50 mg) was dissolved in DI water (5 mL). The lignin solution was added dropwise to the copper solution, heated to 95 °C, and stirred for 3 h, followed by stirring at room temperature for 16 h.

Preparation of the Lignin 5FeNPs.[40] The lignin FeNPs were prepared following the methods in a previous report with minor modifications. An aqueous solution of 20 mg/mL lignin was prepared by adding the lignin (100 mg) to DI water (5 mL) and vortexing and sonicating until it was fully dissolved. In parallel, $Fe(ClO_4)_3)\cdot xH_2O$ (50 mg) was dissolved in DI water (5 mL). The lignin solution was added dropwise to the iron solution and stirred at room temperature for 24 h.

Preparation of the Lignin 5NiNPs. An aqueous solution of 20 mg/mL lignin was prepared by adding the lignin (100 mg) to DI water (5 mL) and vortexing and sonicating until it was fully dissolved. In parallel, $Ni(NO_3)_2\cdot 6H_2O$ (50 mg) was dissolved in DI water (5 mL). The lignin solution was added dropwise to the nickel solution and stirred at room temperature for 3 h.

Preparation of the Lignin ZnNPs. An aqueous solution of 20 mg/mL lignin was prepared by adding the lignin (100 mg) to DI water (5 mL) and vortexing and sonicating until it was fully dissolved. In parallel, $Zn(NO_3)_2\cdot 6H_2O$ (50 mg) was dissolved in DI water (5 mL). The lignin solution was added dropwise to the nickel solution and stirred at room temperature for 3 h.

Preparation of the Lignin-Based Hydrogels. The lignin-based hydrogels were prepared using three different methods: Method A: PAA (200 mg), water (1.0 mL), APS (0.5 mL, 1 wt %) and lignin 5metal NPs (0.5 mL) (the number before the metal corresponds to the concentration of the metal NPs used; 0.5 mL gives a final concentration of 1.25 mg/mL metal NPs in the hydrogel). The PAA was dissolved in the water (20 wt %), and the solution was mixed well by vortex and degassed with nitrogen gas for 5 min. In parallel, solutions of APS and lignin 5metal NPs were freshly prepared. The lignin 5metal NPs (0.5 mL) and APS (0.5 mL, 1 wt %) solutions were added to the PAA (20 wt %) mixture, which was immediately mixed by vortex and then sonicated for 30 s. The mixture was then incubated at room temperature for 1−16 h, resulting in a tough, self-standing hydrogel. Method B: PAA (200 mg), water (0.5 mL), APS (0.5 mL, 1 wt %), and lignin 5metal NPs (1 mL) (1 mL gives a final concentration of 2.5 mg/mL metal NPs in the hydrogel) were used. The PAA was dissolved in the water, and 1 mL of the lignin 5metal NPs was added. Subsequently, the material was mixed well by vortex and degassed with nitrogen gas for 5 min. In parallel, an APS (1 wt %) solution was freshly prepared. This was added to the PAA mixture, which was immediately mixed by vortex and then sonicated for 30 s. The mixture was then incubated at room temperature for 1−16 h, resulting in a tough, self-standing hydrogel. Method C: PAA (200 mg), lignin 5metal NPs (1 mL) (giving a final concentration of 2.5 mg/mL metal NPs in the hydrogel), metal salt (0.5 mL, 1 wt %), and APS (0.5 mL, 1 wt %) were used. The PAA was dissolved in 1 mL of lignin 5metal NPs solution. Subsequently, the material was mixed well by vortex and degassed with nitrogen gas for 5 min. In parallel, an APS (1 wt %) solution and metal salt solution (1 wt %) were freshly prepared. The metal salt (0.5 mL, 1 wt %) and APS (0.5 mL, 1 wt %) solutions were added to the PAA mixture, immediately mixed by vortex and then sonicated for 30 s. The mixture was then incubated at room temperature for 1−16 h.

Preparation of the PAA-Based Hydrogel. The PAA hydrogel was prepared by dissolving the PAA (200 mg) in 1 mL of water, mixing by vortex, and degassing with nitrogen gas for 5 min. In parallel, APS (1 wt %) and $AgNO_3$ (1 wt %) solutions were freshly prepared. The $AgNO_3$ (0.5 mL, 1 wt %) and APS (0.5 mL, 1 wt %) solutions were added to the PAA mixture, which was immediately mixed by vortex and then sonicated for 30 s. The mixture was then incubated at room temperature for 1−16 h.

Electron Paramagnetic Resonance analysis. The experiments were carried out on a Bruker EMX-microspectrometer equipped with an EMX-Premium bridge and an ER4119HS resonator. Each sample was placed in a capillary tube (internal diameter 1.35 mm) which was sealed with a clay plug in one end. The recording settings were: microwave frequency, 9.9 GHz; microwave power, 5 mW; modulation frequency, 100 kHz; modulation amplitude, 5 G; detector receiving gain, 58 dB; time constant, 10.24 ms; and conversion time, 40.96 ms with a spectral resolution of 1024 data points; otherwise ambient conditions were used. The samples were freshly prepared and immediately measured.

EPR Simulation Analysis. EPR simulation was carried out on a Bruker-Xsophe/XeprView software package (v.1.1.4), using spin Hamiltonian $H = g\mu_B BS + AS \times I$, where the first term represents the Zeeman effect, while the second term describes the nuclear hyperfine interaction, treated as a first-order perturbation. For the sake of simplicity, the ^{13}C isotope effect is omitted, and only isotropic super hyperfine interaction of two chemically equivalent ^1H are considered. The resulting parameters are $g = 2.0044$ and $A = 16.5 \times 10^{-4}$ cm^{-1}.

Fourier Transform Infrared Spectrometry. The FTIR analysis was carried out on a Bruker Tensor 27 and was used to analyze the chemical groups in the various materials under controlled atmospheric conditions and in transmittance mode. The spectra were collected at regions between 4000 and 400 cm^{-1}.

https://dx.doi.org/10.1021/acsnano.0c06346
ACS Nano XXXX, XXX, XXX−XXX

UV−visible Absorbance. The measurements were carried out on an Agilent 8453 UV−vis spectrophotometer and recorded between 200 and 800 nm.

Scanning Electron Microscopy. The scaffold morphology characterization was carried out using an FEG SEM instrument (Zeiss, Leo Gemini 1530) at an accelerating voltage of 3 kV. Before the analysis, the hydrogels were lyophilized, and the samples were prepared using two different approaches: directly analyzed in powder form or deployed as a solution and then allowed to dry in the oven.

Scanning Transmission Electron Microscopy. The analysis was carried out using a JEOL 2100F microscope operated at 200 kV and equipped with a Schottky field-emission gun and an ultrahigh-resolution pole piece (C_s = 0.5 mm). The samples (lignin 5AgNPs and lignin 1.25 AgNPs-PAA) were dispersed in DI water and then deposited on a Cu TEM supporting grid with holey carbon films. Bright-field (BF) and high-angle annular dark-field (HAADF) STEM images were simultaneously acquired using the Gatan Microscopy Suite with the Gatan BF or the JEOL ADF detector, respectively.

X-ray Photoelectron Spectroscopy. The oxidation state of the silver within the lignin 5AgNPs was determined with XPS analysis. The XPS spectra were recorded on an ESCA instrument (Physical Electronics, USA).

Rheological Analysis. Samples were stored at room temperature until characterized with an AR-G2 Rheometer (TA Instruments Advanced Rheometer 2000). Hydrogels (4 mm height, 20 mm diameter) were prepared for the tests. The storage (G') and loss modulus (G'') were registered using a titanium plate (19 mm diameter) with a gap of 2500 μm. Samples were loaded onto the plate and allowed to equilibrate for 1 min. For oscillatory rheology, the linear viscoelasticity regimen was confirmed by conducting oscillatory stress sweeps at ∼0.1−1000 Pa and 1 Hz, and an oscillatory frequency sweep was performed at 0.1−100 Hz and 10 Pa. The G' and G'' *versus* shear stress and *versus* angular frequency were registered. All the tests were conducted at 37 °C.

Dynamic Light Scattering Analysis. The NP sizes were characterized using a ZETASIZER Nano Series Nano-ZS MALVERN INSTRUMENTS. All measurements were conducted at 25 °C with at least three replicates.

X-ray Diffraction Analysis. The lignin 5AgNPs sample was characterized using powder XRD (on a Bruker Focus D8 diffractometer with Cu Kα X-ray radiation (λ = 1.54 Å)) analysis. Before the analysis, the lignin 5AgNPs solutions were freeze-dried.

Cyclic Voltammetry analysis. The experiments were carried out to monitor the redox reactions in the materials. The materials of interest (lignin 1.25AgNPs-PAA and PAA) were used as the working electrode, Ag/AgCl (KCl sat.) was the reference electrode, and Pt was the counter electrode. An aqueous solution of PAA (2 wt %) and APS (1 wt %) was used as the electrolyte solution. The CV measurements were carried out at 5 mV s^{-1} between −0.20 and 0.80 V *versus* Ag/AgCl (Figure S6).

The Mechanical Properties. The experiments were carried out using a Shimadzu (AUTOGRAPH AGS-X) mechanical tester with a 500 N load cell. The hydrogels were molded into cylindrical specimens (diameter = 20 mm and height = 8 mm) for compression tests and samples with the dimensions 20 × 5 x 1 mm for tensile tests. The compression and tensile tests were carried out at a speed of 10 mm/min. For the compression test, the material was compressed to 90% of the original height. The cyclic compression tests were performed with the same parameters for six consecutive cycles. The results of the compression and tensile tests were based on the average of five measurements. The maximum compression stress was obtained at the maximum compression on the first cycle, and the compressive modulus was determined from the slope of the stress−strain curve. The ultimate tensile stress was obtained at the failure point, and the elastic modulus was determined from the slope of the stress−strain curve. The energy loss was calculated for the first cycle based on the area between the loading and unloading curves, as in eq 1:[67]

$$\text{energy loss} = \frac{\text{area below loading}}{\text{area below loading} + \text{area below unloading}} \quad (1)$$

Adhesion Property Testing. Lap shear experiments were carried out on Shimadzu equipment according to the modified ASTM F2255-05 standard lap shear strength property of tissue adhesives to measure the strength of adhesion of the hydrogels to various surfaces (glass, steel, and tissue). Two pieces of fresh porcine skin purchased from a local store were cut into samples of 40 mm length, 25 mm width, and 1 mm thickness. These two pieces were glued separately using super glue to glass slides (75 × 25 mm) or steel slides (75 × 25 mm; prepared at the University workshop). The hydrogels (∼50 mg) were applied to the surface of one of the skin specimens with a bond area of 5 cm^2 (20 × 25 mm), and the second specimen was immediately placed over the gel. Force was applied using a clamp for 5 min at 37 °C in a wet environment prior to measurement (Figure S8). The results of the adhesion tests were based on the average of five measurements. The samples were then pulled apart until failure with a cross-head speed of 10 mm/min. The adhesion strengths were calculated as the measured maximum load divided by the bonded area.

Antibacterial Study-Colony Count Assays. The experiments were carried out using the bacterial strains Gram-positive *S. aureus* and Gram-negative *E. coli* for all experiments. BHI broth was inoculated with *S. aureus* and *E. coli* and stored overnight at 37 °C with shaking (100 rpm). Subsequently, a 5 mL sample of the bacterial solution (∼6 × 10^7 CFU/mL) was prepared. To this solution, 50 mg of the hydrogel samples was added and incubated for 24 h at 37 °C under shaking (100 rpm). A 100 μL aliquot was then removed from each sample, and the colony-forming unit (CFU) was determined using serial dilutions and plating on BHI Broth agar plates.

Elution Antibacterial Study-Colony Count Assays. The experiments were carried out following the same procedure as above; however, prior to the addition of the bacteria, the hydrogels were incubated in growth media at 37 °C under shaking (100 rpm) for 24 h. Subsequently, the hydrogels were removed from the growth media, and the remaining solution was used for the antibacterial evaluation.

Ag^+ Release Study. The release study experiments were performed on all the devised hydrogels and quantified through an inductively coupled plasma optical emission spectroscopy (ICP-OES) (AVIO 200 ICP-OES, PerkinElmer). The *in vitro* release experiments were performed by placing 300 mg of the respective hydrogels in a vial containing 2 mL of PBS (pH 7.4) at 37 °C under shaking (100 rpm). At the selected time points, the released PBS was collected and replaced by fresh PBS. The tests were performed in triplicates.

Cellular Viability Test. The cytotoxicity of the engineered hydrogels was evaluated by seeding 3T3 fibroblasts (10 × 10^3) into 96-well culture plates (Corning Inc., Corning, NY) and incubating them with different concentrations (ranging between 0.001 and 1000 g/mL) of PAA, lignin 5AgNPs, lignin 10AgNPs, lignin 1.25AgNPs-PAA, and lignin 2.5AgNPs-PAA for 48 h. A PrestoBlue Cell Viability assay (Thermo Fisher Scientific, Waltham, MA) was employed, and cytotoxicity was measured *via* a microplate reader (Infinite M200 Tecan, Männedorf, Switzerland) and analyzed using i-control software (Tecan, Männedorf, Switzerland).

Statistical Analysis. All experiments were conducted in triplicate or quintuplicate (repeated at least three times) and analyzed using analysis of variance (ANOVA) followed by Tukey's multiple comparisons test to determine statistical differences between mean values.

ASSOCIATED CONTENT

Supporting Information

The Supporting Information is available free of charge at https://pubs.acs.org/doi/10.1021/acsnano.0c06346.

Figure S1: EPR evaluation of the various reactions and components. Figure S2: The spectra of the EPR simulation corroborating the presence of the radical $^{\bullet}CH_2$ species. Figure S3: Images of the screening studies evaluating the success of the cross-linking and tissue

https://dx.doi.org/10.1021/acsnano.0c06346
ACS Nano XXXX, XXX, XXX−XXX

adhesive hydrogels. Figure S4: The preparation of various lignin metal NPs and the NPs sizes. Figure S5: FTIR of the lignin 5AgNPs, lignin, and $AgNO_3$ samples. Figure S6: The experimental setup and parameters used for the electrochemical cell in CV experiments. Figure S7: Self-mending quantification and photo demonstrating the elasticity of the engineered hydrogel. Figure S8: Illustration of the test setup to measure the adhesion of the hydrogels onto various surfaces. Figure 9: The antibacterial activity of the engineered hydrogels against *S. aureus* and *E. coli* in the elution experiment. Figure S10: The Ag^+ release profile from the engineered hydrogels. Figure S11: The cytotoxicity of the various compositions. Table S1: Screening studies for engineering the hydrogel. Scheme S1: The possible radicals formed from AA when treated with APS. Scheme S2: The mechanism of the free radical polymerization of AA. Scheme S3: The mechanism of the Ag-catalyzed oxidative decarboxylation promoting intermolecular cross-linking of PAA. Scheme S4: The mechanism of the decarboxylation reaction of COOH-containing monomers (PDF)

AUTHOR INFORMATION

Corresponding Authors

Samson Afewerki − *Division of Nanotechnology and Functional Materials, Department of Materials Science and Engineering, Ångström Laboratory, Uppsala University, 751 03 Uppsala, Sweden;* orcid.org/0000-0002-5108-6487; Email: samsonafewerki20@gmail.com

Chao Xu − *Division of Nanotechnology and Functional Materials, Department of Materials Science and Engineering, Ångström Laboratory, Uppsala University, 751 03 Uppsala, Sweden;* orcid.org/0000-0002-5342-3686; Email: chao.xu@angstrom.uu.se

Maria Strømme − *Division of Nanotechnology and Functional Materials, Department of Materials Science and Engineering, Ångström Laboratory, Uppsala University, 751 03 Uppsala, Sweden;* orcid.org/0000-0002-5496-9664; Email: maria.stromme@angstrom.uu.se

Authors

Xichi Wang − *Division of Engineering in Medicine, Department of Medicine, Brigham and Women's Hospital, Harvard Medical School, Boston, Massachusetts 02115, United States; Division of Health Sciences and Technology, Harvard University − Massachusetts Institute of Technology (MIT), Cambridge, Massachusetts 02139, United States*

Guillermo U. Ruiz-Esparza − *Division of Engineering in Medicine, Department of Medicine, Brigham and Women's Hospital, Harvard Medical School, Boston, Massachusetts 02115, United States; Division of Health Sciences and Technology, Harvard University − Massachusetts Institute of Technology (MIT), Cambridge, Massachusetts 02139, United States*

Cheuk-Wai Tai − *Department of Materials and Environmental Chemistry, Arrhenius Laboratory, Stockholm University, SE-10691 Stockholm, Sweden*

Xueying Kong − *Division of Nanotechnology and Functional Materials, Department of Materials Science and Engineering, Ångström Laboratory, Uppsala University, 751 03 Uppsala, Sweden*

Shengyang Zhou − *Division of Nanotechnology and Functional Materials, Department of Materials Science and Engineering, Ångström Laboratory, Uppsala University, 751 03 Uppsala, Sweden;* orcid.org/0000-0003-1032-6314

Ken Welch − *Division of Nanotechnology and Functional Materials, Department of Materials Science and Engineering, Ångström Laboratory, Uppsala University, 751 03 Uppsala, Sweden;* orcid.org/0000-0003-4543-1130

Ping Huang − *Department of Chemistry, Ångström Laboratory, Uppsala University, 751 03 Uppsala, Sweden*

Rhodel Bengtsson − *Department of Materials Science and Engineering, Applied Mechanics, Ångström Laboratory, Uppsala University, 751 03 Uppsala, Sweden*

Complete contact information is available at: https://pubs.acs.org/10.1021/acsnano.0c06346

Notes

The authors declare no competing financial interest.

ACKNOWLEDGMENTS

We gratefully acknowledge the Division of Applied Mechanics at the Ångström Laboratory for providing us with the mechanical tester. The Polymer Chemistry division is gratefully acknowledged for letting us use the rheometer, as is Jan Bohlin for helping to set up the tests. The Knut and Alice Wallenberg Foundation is gratefully acknowledged for an equipment grant for the electron microscopy facilities at Stockholm University. C.X. acknowledges the Åforsk research grant (19-493). The EPR service center at Uppsala University is acknowledged for instrument access.

REFERENCES

(1) Aguado, B. A.; Grim, J. C.; Rosales, A. M.; Watson-Capps, J. J.; Anseth, K. S. Engineering Precision Biomaterials for Personalized Medicine. *Sci. Transl. Med.* **2018**, *10*, No. eaam8645.

(2) Uludağ, H. Grand Challenges in Biomaterials. *Front. Bioeng. Biotechnol.* **2014**, *2*, 43.

(3) Davis, S. J.; Caldeira, K.; Matthews, H. D. Future CO_2 Emissions and Climate Change from Existing Energy Infrastructure. *Science* **2010**, *329*, 1330−11333.

(4) Wiedmann, T. Eutrophication's Neglected Drivers. *Nat. Sustain.* **2018**, *1*, 273−274.

(5) Roope, L. S. J.; Smith, R. D.; Pouwels, K. B.; Buchanan, J.; Abel, L.; Eibich, P.; Butler, C. C.; Tan, P. S.; Walker, A. S.; Robotham, J. V.; Wordsworth, S. The Challenge of Antimicrobial Resistance: What Economics Can Contribute. *Science* **2019**, *364*, No. eaau4679.

(6) Afewerki, S.; Bassous, N.; Harb, S.; Palo-Nieto, C.; Ruiz-Esparza, G. U.; Marciano, F. R.; Webster, T. J.; Furtado, A. S. A.; Lobo, A. O. Advances in Dual Functional Antimicrobial and Osteoinductive Biomaterials for Orthopedic Applications. *Nanomedicine* **2020**, *24*, 102143.

(7) Anastas, P. T.; Warner, J. C. *Green Chemistry: Theory and Practice*; Oxford University Press: New York, 1998.

(8) Anastas, P.; Eghbali, N. Green Chemistry: Principles and Practice. *Chem. Soc. Rev.* **2010**, *39*, 301−312.

(9) Sheldon, R. A. Engineering a More Sustainable World through Catalysis and Green Chemistry. *J. R. Soc., Interface* **2016**, *13*, 20160087.

(10) Zhang, X.; Fevre, M.; Jones, G. O.; Waymouth, R. M. Catalysis as an Enabling Science for Sustainable Polymers. *Chem. Rev.* **2018**, *118*, 839−885.

(11) Richter, M.; Schulenburg, C.; Jankowska, D.; Heck, T.; Faccio, G. Novel Materials through Nature's Catalysts. *Mater. Today* **2015**, *18*, 459−467.

(12) Höfer, R.; Bigorra, J. Biomass-Based Green Chemistry: Sustainable Solutions for Modern Economies. *Green Chem. Lett. Rev.* **2008**, *1*, 79−97.
(13) Brun, N.; Hesemann, P.; Esposito, D. Expanding the Biomass Derived Chemical Space. *Chem. Sci.* **2017**, *8*, 4724−4738.
(14) Kirchherr, J.; Reike, D.; Hekkert, M. Conceptualizing the Circular Economy: An Analysis of 114 Definitions. *Resour. Conserv. Recycl.* **2017**, *127*, 221−232.
(15) Kiser, B. Circular Economy: Getting the Circulation Going. *Nature* **2016**, *531*, 443.
(16) Upton, B. M.; Kasko, A. M. Strategies for the Conversion of Lignin to High-Value Polymeric Materials: Review and Perspective. *Chem. Rev.* **2016**, *116*, 2275−2306.
(17) Ahn, B. K. Perspectives on Mussel-Inspired Wet Adhesion. *J. Am. Chem. Soc.* **2017**, *139*, 10166−10171.
(18) Dong, X.; Dong, M.; Lu, Y.; Turley, A.; Jin, T.; Wu, C. Antimicrobial and Antioxidant Activities of Lignin From Residue of Corn Stover to Ethanol Production. *Ind. Crops Prod.* **2011**, *34*, 1629−1634.
(19) Lochab, B.; Shukla, S.; Varma, I. K. Naturally Occurring Phenolic Sources: Monomers and Polymers. *RSC Adv.* **2014**, *4*, 21712−21752.
(20) Zhan, K.; Kim, C.; Sung, K.; Ejima, H.; Yoshie, N. Tunicate-Inspired Gallol Polymers for Underwater Adhesive: A Comparative Study of Catechol and Gallol. *Biomacromolecules* **2017**, *18*, 2959−2966.
(21) Wang, Z.; Zhao, S.; Song, R.; Zhang, W.; Zhang, S.; Li, J. The Synergy between Natural Polyphenol-Inspired Catechol Moieties and Plant Protein-Derived Bio-Adhesive Enhances the Wet Bonding Strength. *Sci. Rep.* **2017**, *7*, 9664.
(22) Krogsgaard, M.; Nue, V.; Birkedal, H. Mussel-Inspired Materials: Self-Healing through Coordination Chemistry. *Chem. - Eur. J.* **2016**, *22*, 844−857.
(23) Mehdizadeh, M.; Weng, H.; Gyawali, D.; Tang, L.; Yang, J. Injectable Citrate-Based Mussel-Inspired Tissue Bioadhesives with High Wet Strength for Sutureless Wound Closure. *Biomaterials* **2012**, *33*, 7972−7983.
(24) Krogsgaard, M.; Andersen, A.; Birkedal, H. Gels and Threads: Mussel-Inspired One-Pot Route to Advanced Responsive Materials. *Chem. Commun.* **2014**, *50*, 13278−13281.
(25) Lang, N.; Pereira, M. J.; Lee, Y.; Friehs, I.; Vasilyev, N. V.; Feins, E. N.; Ablasser, K.; O'Cearbhaill, E. D.; Xu, C.; Fabozzo, A.; et al. A Blood-Resistant Surgical Glue for Minimally Invasive Repair of Vessels and Heart Defects. *Sci. Transl. Med.* **2014**, *6*, 218ra6.
(26) Li, J.; Celiz, A.; Yang, J.; Yang, Q.; Wamala, I.; Whyte, W.; Seo, B.; Vasilyev, N.; Vlassak, J.; Suo, Z.; et al. Tough Adhesives for Diverse Wet Surfaces. *Science* **2017**, *357*, 378−381.
(27) Wirthl, D.; Pichler, R.; Drack, M.; Kettlguber, G.; Moser, R.; Gerstmayr, R.; Hartmann, F.; Bradt, E.; Kaltseis, R.; Siket, C. M.; et al. Instant Tough Bonding of Hydrogels for Soft Machines and Electronics. *Sci. Adv.* **2017**, *3* (6), No. e1700053.
(28) De Paula, M. M. M.; Bassous, N. J.; Afewerki, S.; Harb, S. V.; Ghannadian, P.; Marciano, F. R.; Viana, B. C.; Tim, C. R.; Webster, T. J.; Lobo, A. O. Understanding the Impact of Crosslinked PCL/PEG/GelMA Electrospun Nanofibers on Bactericidal Activity. *PLoS One* **2018**, *13*, No. e0209386.
(29) Afewerki, S.; Córdova, A. Combinations of Aminocatalysts and Metal Catalysts: A Powerful Cooperative Approach in Selective Organic Synthesis. *Chem. Rev.* **2016**, *116*, 13512−13570.
(30) Cremaldi, J. C.; Bhushan, B. Bioinspired Self-Healing Materials: Lessons from Nature. *Beilstein J. Nanotechnol.* **2018**, *9*, 907−935.
(31) Saiz-Poseu, J.; Mancebo-Aracil, J.; Nador, F.; Busqué, F.; Ruiz-Molina, D. The Chemistry behind Catechol-Based Adhesion. *Angew. Chem., Int. Ed.* **2019**, *58*, 696−714.
(32) Gan, D.; Xing, W.; Jiang, L.; Fang, J.; Zhao, C.; Ren, F.; Fang, L.; Wang, K.; Lu, X. Plant-Inspired Adhesive and Tough Hydrogel Based on Ag-Lignin Nanoparticles-Triggered Dynamic Redox Catechol Chemistry. *Nat. Commun.* **2019**, *10*, 1487.
(33) Gan, D.; Shuai, T.; Wang, X.; Huang, Z.; Ren, F.; Fang, L.; Wang, K.; Xie, C.; Lu, X. Mussel-Inspired Redox-Active and Hydrophilic Conductive Polymer Nanoparticles for Adhesive Hydrogel Bioelectronics. *Nano-Micro Lett.* **2020**, *12*, 169.
(34) Anderson, J. M.; Kochi, J. K. Silver(I)-Catalyzed Oxidative Decarboxylation of Acids by Peroxydisulfate. Role of Silver(II). *J. Am. Chem. Soc.* **1970**, *92*, 1651−1659.
(35) Weng, G.; Huang, Y.; Thanneeru, S.; Li, H.; Alamri, A.; He, J. Cross-Linking of COOH-Containing Polymers Using Ag (I)-Catalyzed Oxidative Decarboxylation in Aqueous Solution. *Soft Matter* **2017**, *13*, 5028−5037.
(36) Milczarek, G.; Rebis, T.; Fabianska, J. One-Step Synthesis of Lignosulfonate-Stabilized Silver Nanoparticles. *Colloids Surf., B* **2013**, *105*, 335−341.
(37) Coccia, F.; Tonucci, L.; Bosco, D.; Bressan, M.; d'Alessandro, N. One-Pot Synthesis of Lignin-Stabilised Platinum and Palladium Nanoparticles and Their Catalytic Behaviour in Oxidation and Reduction Reactions. *Green Chem.* **2012**, *14*, 1073−1078.
(38) Marulasiddeshwara, M.; Kumar, P. R. Synthesis of Pd (0) Nanocatalyst Using Lignin in Water for the Mizoroki−Heck Reaction under Solvent-Free Conditions. *Int. J. Biol. Macromol.* **2016**, *83*, 326−334.
(39) Li, P.; Lv, W.; Ai, S. Green and Gentle Synthesis of Cu2O Nanoparticles Using Lignin as Reducing and Capping Reagent with Antibacterial Properties. *J. Exp. Nanosci.* **2016**, *11*, 18−27.
(40) Zhang, Q.; Li, M.; Guo, C.; Jia, Z.; Wan, G.; Wang, S.; Min, D. Fe3O4 Nanoparticles Loaded on Lignin Nanoparticles Applied as a Peroxidase Mimic for the Sensitively Colorimetric Detection of H_2O_2. *Nanomaterials* **2019**, *9*, 210.
(41) Dizhbite, T.; Telysheva, G.; Jurkjane, V.; Viesturs, U. Characterization of the Radical Scavenging Activity of Lignins-Natural Antioxidants. *Bioresour. Technol.* **2004**, *95*, 309−317.
(42) García, A.; González Alriols, M.; Spigno, G.; Labidi, J. Lignin as Natural Radical Scavenger. Effect of the Obtaining and Purification Processes on the Antioxidant Behaviour of Lignin. *Biochem. Eng. J.* **2012**, *67*, 173−185.
(43) Kolthoff, I. M.; Miller, I. K. The Chemistry of Persulfate. I. The Kinetics and Mechanism of the Decomposition of the Persulfate Ion in Aqueous Medium. *J. Am. Chem. Soc.* **1951**, *73*, 3055−3059.
(44) Paidikondala, M.; Wang, S.; Hilborn, J. n.; Larsson, S.; Varghese, O. P. Impact of Hydrogel Cross-Linking Chemistry on the *in Vitro* and *in Vivo* Bioactivity of Recombinant Human Bone Morphogenetic Protein-2. *ACS Appl. Bio Mater.* **2019**, *2*, 2006−2012.
(45) Vanderhooft, J. L.; Mann, B. K.; Prestwich, G. D. Synthesis and Characterization of Novel Thiol-Reactive Poly (ethylene Glycol) Cross-Linkers for Extracellular-Matrix-Mimetic Biomaterials. *Biomacromolecules* **2007**, *8*, 2883−2889.
(46) Rak, M. J.; Friščić, T.; Moores, A. Mechanochemical Synthesis of Au, Pd, Ru and Re Nanoparticles with Lignin as a Bio-Based Reducing Agent and Stabilizing Matrix. *Faraday Discuss.* **2014**, *170*, 155−167.
(47) Menter, P. Acrylamide Polymerization − A Practical Approach. *Bio-Rad Tech Note 1156*; Bio-Rad Laboratories: Hercules, CA, 2000; p 24
(48) Jeyaraj, M.; Praphakar, R. A.; Rajendran, C.; Ponnamma, D.; Sadasivuni, K. K.; Munusamy, M. A.; Rajan, M. Surface Functionalization of Natural Lignin Isolated from Aloe Barbadensis Miller Biomass by Atom Transfer Radical Polymerization for Enhanced Anticancer Efficacy. *RSC Adv.* **2016**, *6*, 51310−51319.
(49) Zhong, M.; Liu, Y.-T.; Liu, X.-Y.; Shi, F.-K.; Zhang, L.-Q.; Zhu, M.-F.; Xie, X.-M. Dually Cross-Linked Single Network Poly (acrylic Acid) Hydrogels with Superior Mechanical Properties and Water Absorbency. *Soft Matter* **2016**, *12*, 5420−5428.
(50) Gustafson, R. L.; Lirio, J. A. Binding of Divalent Metal Ions by Crosslinked Polyacrylic Acid. *J. Phys. Chem.* **1968**, *72*, 1502−1505.
(51) Agarwal, U. P., Atalla, R. H. Vibrational Spectroscopy. In *Lignin and Lignans, Advances in Chemistry*; Heitner, C., Dimmel, D. R., Schmidt, J. A., Eds.; CRC Press: Boca Raton, FL, 2010; pp 103−136.

https://dx.doi.org/10.1021/acsnano.0c06346
ACS Nano XXXX, XXX, XXX−XXX

(52) Hu, H.; Saniger, J.; Garcia-Alejandre, J.; Castaño, V. M. Fourier Transform Infrared Spectroscopy Studies of the Reaction between Polyacrylic Acid and Metal Oxides. *Mater. Lett.* **1991**, *12*, 281−285.
(53) Jabbari, E.; Wisniewski, N.; Peppas, N. A. Evidence of Mucoadhesion by Chain Interpenetration at a Poly (acrylic Acid)/Mucin Interface Using ATR-FTIR Spectroscopy. *J. Controlled Release* **1993**, *26*, 99−108.
(54) Anandalakshmi, K.; Venugobal, J.; Ramasamy, V. Characterization of Silver Nanoparticles by Green Synthesis Method Using Pedalium Murex Leaf Extract and Their Antibacterial Activity. *Appl. Nanosci.* **2016**, *6*, 399−408.
(55) Nair, V.; Dhar, P.; Vinu, R. Production of Phenolics *via* Photocatalysis of Ball Milled Lignin−TiO_2 Mixtures in Aqueous Suspension. *RSC Adv.* **2016**, *6*, 18204−18216.
(56) Albarran, G.; Boggess, W.; Rassolov, V.; Schuler, R. H. Absorption Spectrum, Mass Spectrometric Properties, and Electronic Structure of 1,2-Benzoquinone. *J. Phys. Chem. A* **2010**, *114*, 7470−7478.
(57) Rout, Y.; Behera, S.; Ojha, A. K.; Nayak, P. Green Synthesis of Silver Nanoparticles Using Ocimum Sanctum (Tulashi) and Study of Their Antibacterial and Antifungal Activities. *J. Microbiol. Antimicrob.* **2012**, *4*, 103−109.
(58) Milczarek, G. Lignosulfonate-Modified Electrodes: Electrochemical Properties and Electrocatalysis of NADH Oxidation. *Langmuir* **2009**, *25*, 10345−10353.
(59) Milczarek, G. Preparation and Characterization of a Lignin Modified Electrode. *Electroanalysis* **2007**, *19*, 1411−1414.
(60) Weng, L.; Chen, X.; Chen, W. Rheological Characterization of *in Situ* Crosslinkable Hydrogels Formulated from Oxidized Dextran and N-Carboxyethyl Chitosan. *Biomacromolecules* **2007**, *8*, 1109−1115.
(61) Gaharwar, A. K.; Kishore, V.; Rivera, C.; Bullock, W.; Wu, C. J.; Akkus, O.; Schmidt, G. Physically Crosslinked Nanocomposites from Silicate-Crosslinked PEO: Mechanical Properties and Osteogenic Differentiation of Human Mesenchymal Stem Cells. *Macromol. Biosci.* **2012**, *12*, 779−93.
(62) Jones, D. R. H.; Ashby, M. F. Elastic Moduli. In *Engineering Materials 1, An Introduction to Properties, Applications and Design*, 5th ed.; Jones, D. R. H., Ashby, M. F., Eds.; Butterworth-Heinemann Elsevier: Oxford, UK, 2019; pp 31−47.
(63) Carlisle, C. R.; Coulais, C.; Guthold, M. The Mechanical Stress−Strain Properties of Single Electrospun Collagen Type I Nanofibers. *Acta Biomater.* **2010**, *6*, 2997−3003.
(64) Liu, Y.; Lee, B. P. Recovery Property of Double-Network Hydrogel Containing a Mussel-Inspired Adhesive Moiety and Nano-Silicate. *J. Mater. Chem. B* **2016**, *4*, 6534−6540.
(65) Wei, Z.; Yang, J. H.; Zhou, J.; Xu, F.; Zrínyi, M.; Dussault, P. H.; Osada, Y.; Chen, Y. M. Self-Healing Gels Based on Constitutional Dynamic Chemistry and Their Potential Applications. *Chem. Soc. Rev.* **2014**, *43*, 8114−8131.
(66) Hofman, A. H.; van Hees, I. A.; Yang, J.; Kamperman, M. Bioinspired Underwater Adhesives by Using the Supramolecular Toolbox. *Adv. Mater.* **2018**, *30*, 1704640.
(67) Chung, J.; Lachapelle, K.; Wener, E.; Cartier, R.; De Varennes, B.; Fraser, R.; Leask, R. L. Energy Loss, a Novel Biomechanical Parameter, Correlates with Aortic Aneurysm Size and Histopathologic Findings. *J. Thorac. Cardiovasc. Surg.* **2014**, *148*, 1082−1089.

https://dx.doi.org/10.1021/acsnano.0c06346
ACS Nano XXXX, XXX, XXX−XXX